IEEE Access
Multidisciplinary | Rapid Review | Open Access Journal

Received March 28, 2020, accepted May 4, 2020, date of publication May 7, 2020, date of current version May 21, 2020.

Digital Object Identifier 10.1109/ACCESS.2020.2993034

A Battery-Free Temperature Sensor With Liquid Crystal Elastomer Switching Between RFID Chips

YOUSUF SHAFIQ[1], (Member, IEEE), JULIA HENRICKS[2], CEDRIC P. AMBULO[2], TAYLOR H. WARE[2], AND STAVROS V. GEORGAKOPOULOS[1], (Senior Member, IEEE)

[1]Department of Electrical and Computer Engineering, Florida International University, Miami, FL 33174, USA
[2]Department of Bioengineering, The University of Texas at Dallas, Richardson, TX 75080, USA

Corresponding author: Stavros V. Georgakopoulos (georgako@fiu.edu)

This work was supported by the National Science Foundation under Grant ECCS 1711467 and Grant 1711383.

ABSTRACT In this research, we have developed a novel temperature sensor to be utilized in the Cold-Supply-Chain (CSC) for perishable items. This sensor conveys temperature threshold crossings by switching operation between two individual RFID ICs, i.e., two individual Electronic Product Codes (EPCs). The advantage of this sensor compared to other existing technologies is that it can operate passively (i.e., battery-free) through multiple room-to-cold and cold-to-room temperature cycles, in real-time, without requiring any form of resetting. This design utilizes innovative cold-responsive liquid crystal elastomers (LCEs), which change shape when stimulated by cold temperatures and returns to a relaxed state when the stimulus is removed. In fact, this is the first temperature sensor that conveys temperature threshold crossings by switching between two RFID ICs using LCEs. The correct operation of the sensor is validated by RFID measurements. ANSYS HFSS and ANSYS Circuit Designer were used for the simulation analysis. The performance of the proposed design was validated using simulations and measurements.

INDEX TERMS RFID temperature sensor, liquid crystal elastomers (LCEs), passive RFID, multi-chip RFID antenna, bow-tie antenna, microstrip balun.

I. INTRODUCTION

In recent years, the Cold-Supply-Chain (CSC) has grown in demand due to the rising world population, developing nations, technological advancements, and federal regulations which advocate the use of CSC [1]. Moreover, the CSC is critical to the growth of global trade and to the worldwide availability of food and health supplies [2]. As an example of the current demand in the CSC, the current retail food market consists of 65% fresh-food products [3].

When transporting perishable items, it is essential that they are maintained in a controlled temperature environment to minimize metabolic and microbial deterioration or spoilage [4]. Fresh-food products; such as, meats, fruits, and vegetables, experience discoloration and loss of nutrients when exposed to high-temperatures [5]. Also, medicines, such as, insulin and vaccines, can lose potency if they are not kept in the appropriate temperatures [6]. Typically, the required preservation temperatures for such products range from $-1°$ to $10°$ C [5], [6].

The associate editor coordinating the review of this manuscript and approving it for publication was Trivikram Rao Molugu.

The CSC does consist of discrete check-points, where temperature monitoring is conducted, e.g., at the sending and receiving stations, and within the transportation containers [5], [7]. Such temperature measurements are used to assess the overall quality of transported goods. Unfortunately, this method of quality monitoring is limited as it cannot capture all the irregularities that can occur during the CSC [8]. Firstly, extended delay times at the loading and unloading cargo-docks, where exposure to excessive temperature conditions is probable and even short periods of exposure can cause considerable damage [5], [8]. Secondly, operator errors; such as, constantly opening and/or leaving the container doors open, failure to pre-cool the container before loading, and road accidents, can lead to damaged perishable goods. In addition to operator errors, improper placement during loading is crucial as temperature conditions can vary up to 35% within a single pallet of goods [9]. Also, inadequate packaging may prevent items from being maintained at the proper temperature during the delivery cycle [5], [8]. Lastly, in cases of malfunctioning refrigeration equipment (e.g., intermittent functionality), perishable items can arrive damaged without the knowledge of the operator [8]. As a result, 30% of fresh-food

products arrive damaged to the last check-point during transit. The global losses in the food industry equate to more than $750 Billion per year [2], [7], [9]. Moreover, in 2015 the global sales of organic foods totaled to $81.6 Billion and the total sales of biopharmaceuticals totaled to $260 Billion [2], [10] . Due to the safety-risk, high-consumption rate, and financial-risk involved with transporting perishable goods within the CSC an effective sensor solution to monitor such items is critical.

In this research, RFID technology is utilized. This technology is practical as RFID uses a standardized communication protocol that supports purely passive tag designs. Moreover, RFID technology uses non-line-of-sight wireless communication [11, pp. 43-46]. Originally, RFID technology was designed for cataloging and detection of people and/or objects [11, pp. 15-22]. Over the recent years, this technology has expanded to serve sensing applications. Sensing using RFID technology can be acquired in two ways. The first way uses RFID tags with onboard IC sensors. This approach is common among RFID temperature sensors, where the data is collected, digitized and down-linked to the reader. Unfortunately, this type of RFID sensor has the following disadvantages: (a) it requires proprietary decoding software, which adds a layer of complexity within the supply-chain, (b) it has limited operational life since it uses batteries, (c) it is expensive due to its the complex design and (d) it requires maintenance. Furthermore, such sensors serve as data-loggers, which are limited to a finite amount of monitoring data points. Also, they are limited to operate within a certain temperature range. To our knowledge commercially available RFID temperature sensors, such as, the Freshtime semiactive RFID tag from Infratab Inc., the i-Q327 by Identec Solutions, the IDS-SL13A from IDS Microchip AG, the Sensor Temperature Dogbone by Smartrac, and the SL-900A by AMS Technologies, have one or more of these disadvantages, [9], [16], [17]

Due to these limitations of commercially available RFID temperature sensors, a second methodology of sensing using RFID technology is adapted. Specifically, sensing is conducted through controlled variations of the RFID tag's antenna performance [18]–[20]. This methodology is preferred for the following reasons: (a) no additional layer of software is required, (b) it ensures the longevity of the sensor since it is purely passive (or battery-less), (c) it is cost-effective due to the simplicity in the design, (d) it is maintenance-free since no batteries are required, and (e) it provides real-time temperature monitoring so that operators can act quickly to address problems and preserve the quality of perishable goods. For these reasons, this methodology is used in this research.

As mentioned above, RFID sensor designs with separate onboard IC temperature sensors face many challenges. Therefore, it is informative to directly compare the functionalities of a commercial RFID temperature sensor to our proposed design. Table 1 illustrates such a comparison and highlights the advantages of our proposed sensor compared to the SL-900A Sensory Tag Chip by AMS Technologies [16], [17].

TABLE 1. Comparison of our sensor with the SL-900A sensory tag chip by AMS technologies.

Parameter	Developed Sensor in this Research	SL900A
Technology	Passive: Maintenance free and Cost-effective	Active Operation: Uses batteries that require yearly replacement [17] OR Passive Operation: Compromised accuracy due to EM heating [16, p. 14]
Temperature Range	-10° C (Adaptable to any temperature by modifying the design of the LCE)	-29° C to +58° C
Tracking Domain	Continuous Monitoring: Operates in real-time without any resetting	Data-Logger: Limited to a finite amount of temperature storage points (i.e., 841 points)
Sensing Functionality	Using Changes in Antenna Performance	Using an Onboard Sensor IC
Data Accessibility	Any RFID reader can be Utilized: Only EPCs need to be read	Extra Layer of Software is Required to Plot Temperature Data

Thus far, passive RFID temperature sensors that operate through the controlled changes in the antenna performance have been investigated. For example, a sensor whose operating frequency is dependent on the ambient temperature was presented in [21]. This sensor consists of a dipole antenna that is matched to an RFID IC using a combination of meandering transmission lines and a T-matching network. A water-pocket is placed above this matching network. The temperature dependent relative-permittivity of the water is linear and controls the stray capacitance of the meandered lines. This causes temperature-dependent shifts of the tag's operating frequency. Unfortunately, this design was limited to the freezing and boiling temperatures of water. Additionally, an RFID temperature sensor, which switches its operating frequency based on the temperature, was developed in [22]. The design consists of an antenna that uses two patches (each one with a slot and a passive thermal switch), which resonate at slightly different frequencies. However, for any operating state of this sensor, two resonant frequencies exist, and the temperature is determined based on the difference of these two frequencies. Moreover, for one of its operating states, this sensor has a resonant frequency outside the global UHF RFID band of 860-960 MHz. Overall, this design entails many difficulties for a practical implementation.

Furthermore, in [7] and [9], researchers studied passive RFID temperature sensors that detune due to the temperature-dependent repositioning of a ground plane in reference to

an RFID tag. Specifically, in [7], a customized RFID tag switches its operating frequency by actuating a ground plane under a customized RFID tag using a heat-reactive shape memory polymer. In [9], a design is presented that uses a pair of conventional RFID tags along with a shifting ground plane, which is incased in a fluid. When the fluid is in its solid state, only one tag is read, whereas when the fluid melts the ground plane shifts and the other tag is read. Also, a novel RFID based temperature sensor with a substrate of paraffin wax was designed in [23]. As the temperature threshold is reached, the wax melts thereby changing the operating frequency of the RFID tag. Unfortunately, all these sensors require resetting or replacement. Hence, they are not very well suited for the CSC.

Thus far, as presented earlier, many of the passive RFID temperature sensor designs use the re-tuning of the operating frequency of tags to detect changes in temperature. Another approach was presented in [24], which proposed RFID tags that switch operation between multiple embedded RFID ICs. Also, in [25], designers developed a tag with two RFID ICs, one of which is shorted through a wire-switch made from a shape memory alloy (i.e., Nitinol, which is a Nickle-Titanium alloy). This switch reacts to elevated temperatures by morphing into a rigid formation and breaking the shorted connection. This allows the second RFID IC to also be read. Therefore, when two RFID ICs are read from the tag, the user can then infer that a temperature threshold has been crossed. Unfortunately, this design is limited to a single use as well.

All the sensors presented above provide various solutions for monitoring perishable goods in CSC. However, each design has limitations, which can potentially prevent them from being utilized in fast-paced environments, such as the CSC. As a result, we propose the following set of capabilities for the temperature sensor that we will develop here for CSC applications: (a) The sensor should be compact so that it can be installed on items of various sizes. (b) The sensor should operate continuously (i.e., monitor temperatures in a reversible manner, from room-to-cold and cold-to-room temperatures). (c) The sensor should operate independently (i.e., there is no resetting of any kind required and the sensor can operate through multiple room-to-cold and cold-to-room temperature cycles). (d) The design should be purely passive (i.e., battery-free) to ensure longevity, cost-effectiveness, and convenience (i.e., does not require battery or sensor replacement). (e) the design should operate wirelessly so that the sensor can be applied to individual items. Notably, no other current technology can simultaneously support these capabilities. Also, the proposed temperature sensor will be able to monitor the temperature of perishable goods in conditions where the current method of discrete monitoring cannot (i.e., due to the CSC irregularities mentioned earlier). The wireless capability of our sensor should support monitoring many items (i.e., in dense sensor scenarios) in cluttered environments (many EM reflections) at once [11, pp. 68-73, pp. 361-370]. Hence, as mentioned earlier we choose to use RFID technology.

Novel Liquid Crystal Elastomers (LCEs) have been used to design temperature sensors for cold and hot temperatures [26], [27] and reconfigurable antennas [28]. LCEs are programmable stimuli responsive polymers, which return to their original shape once the stimulus is removed. Specifically, in the passive RFID sensor we presented in [26], a 4D printed triangular array of LCE cells was utilized to activate a switch when the temperature dropped below a certain threshold and in turn reversibly shift the operating frequency of the RFID sensor. This design consisted of a customized patch antenna integrated with a slot that was shorted by the mechanical switch. In this research, we incorporate the same LCE triangular array in a completely different sensor design. Specifically, we develop here a new temperature sensor that consists of two RFID ICs. Each IC contains a unique Electronic Product Code (EPC). Based on the temperature, our sensor continuously switches its operation from one RFID IC to the other. This method enables the accurate determination of the ambient temperature conditions and satisfies all the sensor guidelines proposed above. Finally, the temperature threshold for the actuation of LCEs is also controllable.

In addition, we envision each Cold Supply Chain (CSC) delivery vehicle and loading-dock to be equipped with an RFID wireless reader. Also, handheld RFID wireless readers are to be utilized as well. The concept is to monitor each perishable item individually. This will be accomplished by attaching our sensor (which is purely-passive) to each perishable item to conduct temperature monitoring in a continuous (real-time) and independent (i.e., without resetting) fashion. As mentioned earlier, these attributes are obtained by incorporating novel LCEs in our design. Moreover, since each sensor conveys temperature threshold crossings by switching between one of two unique RFID Electronic Product Codes (EPCs), each sensor will come (from the manufacturer) with the unique EPCs that identify the specific temperature states. During processing, each EPC would be uploaded into the RFID reader computing mainframe at which point each item can be monitored wirelessly and an alert will be sent when any item(s) exceeds a temperature threshold.

Furthermore, the above mentioned capabilities of the proposed sensor address the issues of malfunctioning refrigeration equipment (e.g., intermittent functionality) and operator error (i.e., improperly placed items during loading, inadequate packaging, constantly opening and/or leaving the container doors open, and failure to pre-cool the container before loading) because now each item will have a sensor that will continuously and independently relay temperature conditions as opposed to a single discrete reading from the vehicle's thermostat to represent the temperature condition of all items. For example, if the freezer for any reason shuts-off and the perishable items are exposed to harmful temperature conditions then suddenly turns back on, the single thermostat reading conveys only instantaneous information and there is no knowledge of the harmful temperature exposure. However, the developed sensor presented here will continuously and independently monitor the condition of each

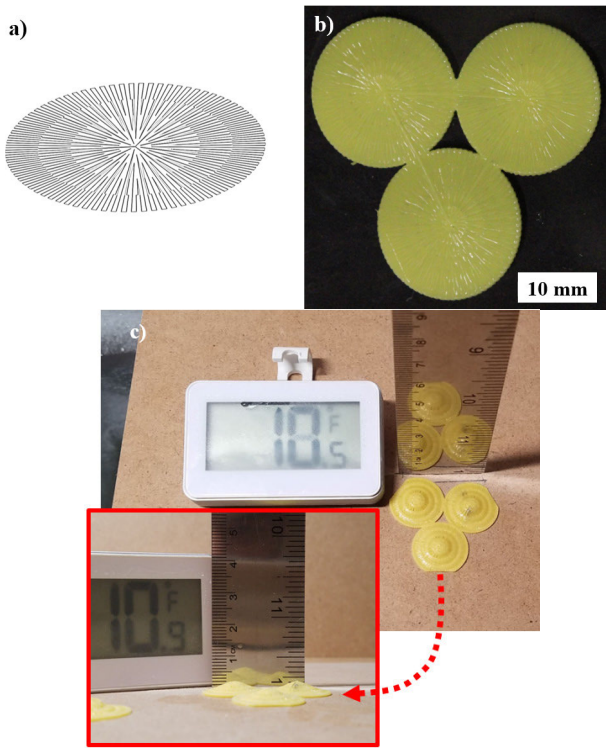

FIGURE 1. a) A schematic of the radial print pattern for each of the disks within the LCE triangular disk array. b) A 3D printed LCE actuator utilized for the sensor design in the relaxed state, c) The LCE actuator is shown in the excited state.

item. Furthermore, since each item will have its own sensor, unacceptable temperature exposures due to extended waiting times at the loading and unloading cargo-docks will be detectable. On the contrary, the current method of discrete point monitoring cannot measure temperatures at these delivery cycle points (i.e., cargo-docks).

In Section II, the details of our novel Liquid Crystal Elastomers (LCEs) are presented. In Section III, the design and functionality of our sensor are described. In Section IV, the 3-port modeling of the mechanical switch is discussed. In Section V the design of the matching networks is presented and in Section VI our sensor's power switching capability is tested. Finally, in Section VII, our sensor's functionality is verified under various environmental conditions.

II. LIQUID CRYSTAL ELASTOMERS

To achieve devices that respond to changes in temperature, liquid crystal elastomers (LCEs) are utilized as soft actuators within this antenna sensor. LCEs are stimuli-responsive polymers that exhibit reversible shape change when exposed to changes in temperature. This response is a result of liquid crystalline phase transitions within the material [29]. To exhibit reversible shape change in the absence of a load, the LCE must be processed so that alignment occurs prior to crosslinking. The resulting material, which most typically exhibits the nematic phase, undergoes a transition into a disordered, isotropic phase on heating causing a macroscopic shape change. Specifically, this phase transition causes a reduction of length along the alignment direction and a smaller expansion along the two directions perpendicular to the alignment direction. This deformation is reversible back to the original programmed state when the thermal stimulus is removed. Researchers utilize alignment processing techniques such as mechanical straining, directed self-assembly, or 3D printing to fabricate these stress-free LCE actuators [30]–[34].

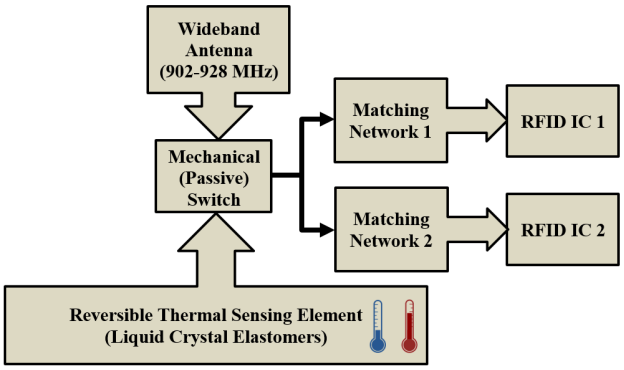

FIGURE 2. Operational diagram of the proposed temperature sensor.

While most LCE soft actuators are activated by controlled heating, cooling also induces anisotropic shape change. Shape change through cooling below the processing temperature has been studied in flat films that twist and in 3D printed conical actuators. In order to achieve coning upon cooling, the LCE must be patterned in a radial manner [35]. Here, we utilize direct ink writing to 3D print an array of 3 LCE disks, each with a radial pattern, refer to Fig. 1(a). The chosen printed LCE chemistry is capable of actuating below 9°C for monitoring of cold-temperature response. A triangular array of connected disks (750 μm thick) was designed and fabricated to provide the necessary force output and displacement to activate the mechanical switch of our RFID tag (0.14 N and 1.5 mm, respectively) upon coning in cold environments. This triangular array is shown in the relaxed and excited states in Figs. 1(b) and 1(c), respectively. The chemistry and printing parameters of the LCE actuators have been previously described in [32].

III. PROPOSED TAG DESIGN

Our RFID sensor tag switches between two Alien Higgs RFID ICs based on the temperature. The internal memory of each IC contains a unique identifying 96-bit Electronic Product Code (EPC) [21]. Therefore, based on this unique identifier, two different temperature thresholds can be clearly detected by switching between two RFID ICs. Moreover, each RFID IC has a sensitivity of -18 dBm and an input impedance of $Z_{IC} = 18 - 164j$ [7], [21], [36], [37].

The functionality of the proposed sensor is best summarized by the diagram shown in Fig. 2. The tag consists of the following three components: the antenna with its balun,

a three-port mechanical (passive) switch, and a set of matching networks.

The proposed sensor consists of a wideband antenna that operates in the RFID UHF band of 902 to 928 MHz. The output of the antenna is fed into a mechanical light-duty switch, which is utilized to keep the design purely passive [38]. Moreover, our novel cold-reactive liquid crystal elastomers are utilized to reversibly trigger the switch upon reaching a temperature threshold. Furthermore, in the relaxed state (at room temperature) the switch is configured to activate the first RFID IC (RFID IC 1). When a temperature threshold is reached, the LCE morphs into a cone shape and activates the switch. As a result, RFID IC 1 is then turned OFF and RFID IC 2 is turned ON. Therefore, by switching between the two RFID ICs, one can easily assess whether a temperature threshold has been reached. Furthermore, since our LCE returns to its original form when the stimulation is removed, the sensor can operate continuously through multiple temperature cycles without the use of any batteries.

A. ANTENNA AND FEED STRUCTURE

In our sensor design, a microstrip coplanar bow-tie antenna is used. This antenna is a lightweight and practical derivative of the infinite biconical antenna [39, pp. 487-496]. Furthermore, the bow-tie antenna retains the wideband constant input-impedance characteristic of the biconical antenna. Specifically, the input impedance of the bow-tie antenna depends on its flare angle and according to Rumsey's principle, an antenna is frequency-independent if the antenna shape can be specified in terms of angles [40]. To design our bow-tie antenna for the RFID UHF band, we used the equations presented in [39, p. 494]. Then, we optimized our design using simulation analysis, which was performed in ANSYS HFSS.

Furthermore, due to the symmetry of the bow-tie dipole, this antenna is balanced [41]. As a result, the feed structure consists of a single-input 50Ω microstrip transmission line connected to a quarter-wave transformer. The output of this transformer behaves as a T-junction and transitions into a pair of 50Ω microstrip transmission lines. Hence, this transformer will translate a 50Ω transmission line impedance into a 35.4Ω transmission line load. The pair of microstrip transmission lines are then designed with a phase difference of 180°. This phase difference generates an odd-mode current excitation, which can be naturally transferred to the symmetric coplanar strip-line (CPS) that feeds the coplanar bow-tie antenna [42]–[45]. The CPS was designed based on the closed-form equations in [46], and then optimized using simulations. The final length of the CPS is $0.365\lambda_g$ (33.35mm). The ratio of the substrate-height to the trace-width is 0.907 and the space between the traces of the CPS is 0.1mm. Based on the equations and design plots presented in [46], these dimensions provide a CPS with a characteristic impedance of approximately 50Ω. Finally, an optimized design using Rogers TMM13i substrate with relative permittivity of 12.85 was simulated [47]. This high permittivity substrate miniaturized the area of the final sensor design to approximately 10 cm × 10 cm, as shown in Fig. 20. Thus, this design is applicable to many shipping crates that typically have sides larger than this area [27], [48].

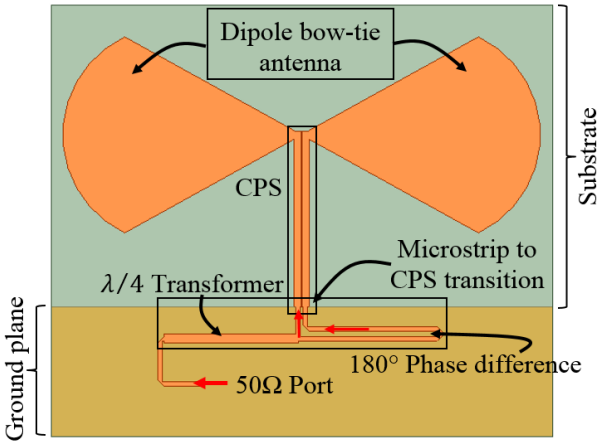

FIGURE 3. Antenna with its feed network.

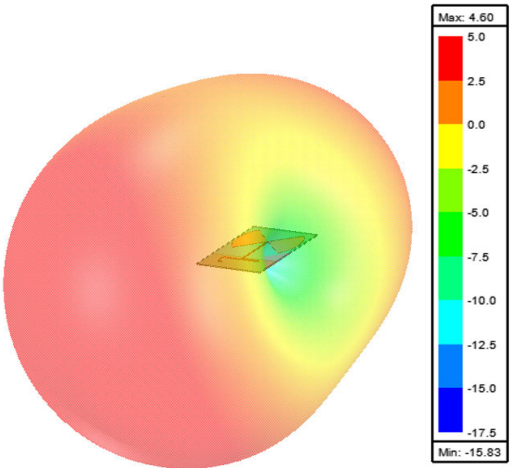

FIGURE 4. Antenna radiation pattern (realized gain in dBi) showing 360° coverage in the elevation-plane.

The antenna and its feed network are shown in Fig. 3. Fig. 4 illustrates the simulated 3-D radiation, which shows that our antenna provides 360° elevation-plane coverage. This is advantageous over patch antenna designs, which only provide coverage in a half-plane opposite to the ground plane. Therefore, the advantage of this design is that when it is placed on various items, the items can be read by the interrogator with less dependence on their orientation (e.g., the antenna does not need to directly face the interrogator).

The proposed antenna design along with its feed network was fabricated and tested as shown in Fig. 5. An SMA connector was soldered to the input of the design. Moreover, an enclosure was designed to elevate the antenna from any resting plane. This elevation prevents the detuning of the antenna when it is placed on various surfaces, such as, wood, plastic, and cardboard.

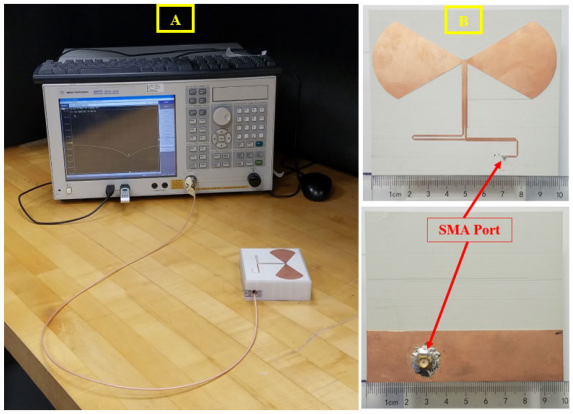

FIGURE 5. VNA test setup with fabricated antenna.

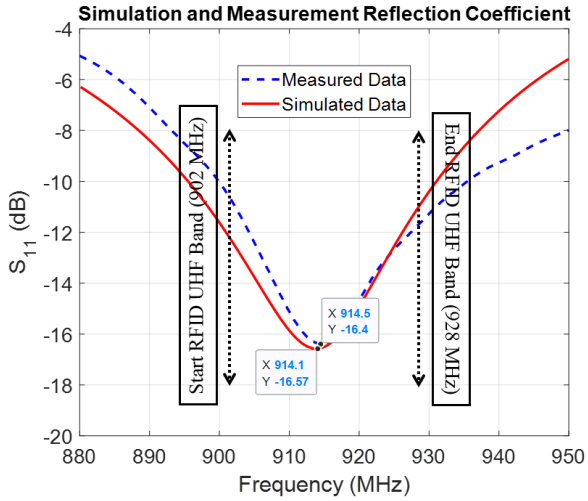

FIGURE 6. Measured and simulated S_{11} of the proposed antenna.

The measured and simulated responses of our antenna are plotted in Fig. 6. The measurement results agree very well with the simulated ones. Also, our antenna provides a good impedance match over the UHF RFID bandwidth, i.e., the reflection coefficient is less than −10 dB from 902 to 928 MHz (this equates to more than 90% power transfer within the frequency-band).

IV. THREE-PORT SWITCH MODEL

In reference to Figs. 2 and 3, the 50Ω port feeds into a passive switch. In our sensor design, we utilize a light-duty mechanical single-pole-double-throw switch, which is made by Omron Electronics [48]. The concept is that the switch will be activated by our newly developed cold-reactive LCEs. Therefore, our sensor's operation is purely passive, temperature dependent, and reversibly functional. However, this switch has been designed to operate at DC. Consequently, a model of the switch's RF performance must be developed in the RFID UHF band, which must be included in our simulation analysis. Our procedure for deriving this model is discussed in what follows.

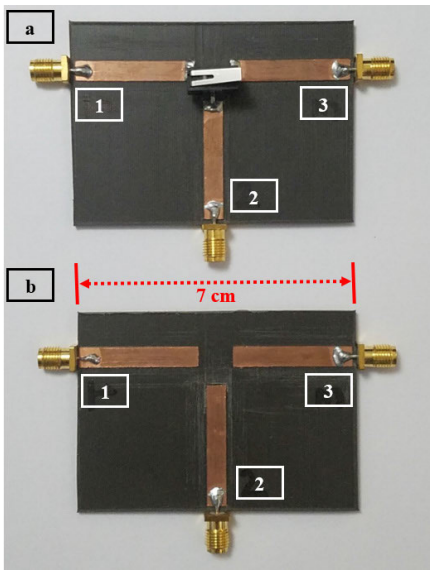

FIGURE 7. Mechanical switch testing circuit. (a) Mechanical switch with de-embedding circuit. (b) De-embedding circuit for electrical length compensation.

Initially, a de-embedding circuit is fabricated. The circuit consists of the switch with each terminal connected to a transmission line, which is terminated to an SMA port, as shown in Fig. 7(a). Additionally, an identical circuit is made without the switch to compensate for the electrical length of the transmission lines (i.e., set the reference planes exactly at the terminals of the switch), as shown in Fig. 7(b). The electrical lengths of transmission lines are calculated by using the open-circuit auto port-extension feature of the E5061B Vector Network Analyzer (VNA).

Since our switch is passive, it has S-parameters that are reciprocal, i.e., $S_{ij} = S_{ji}$, [50, p. 175]. Using the design in Fig. 7(b), an open-circuit auto port-extension is conducted while connected to two ports; for example, ports 1 and 2. Subsequently, this circuit is disconnected and the circuit from Fig. 7(a) is connected to the corresponding ports (i.e., ports 1 and 2). The third remaining port is terminated into a 50Ω load. The 2-port S-parameters are then measured. This process is repeated for ports 1 and 3, and ports 2 and 3. These three 2-port measurement sets are then combined to form a single 3-port touchstone file. This file is used as our switch's model and it is imported in ANSYS Circuit Designer. Notably, the three measurements mentioned above are conducted for both activated (ON) and de-activated (OFF) states of the switch. The switch's insertion losses are plotted in Fig. 8 for both states.

V. MATCHING NETWORK DESIGN

According to our sensor's design (see Fig. 2) an RFID IC needs to be connected to each of the terminals of the switch. However, before placing each IC, an appropriate matching network must be designed. Our objective here is to design a pair of matching networks (at the output of each

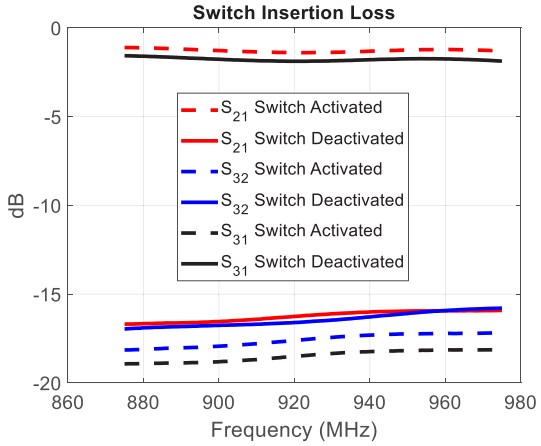

FIGURE 8. Insertion losses of the 3-port mechanical switch for the deactivated and activated states.

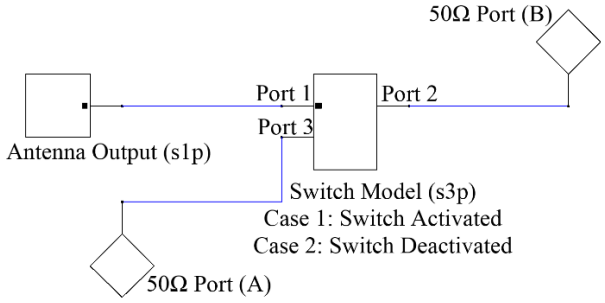

FIGURE 9. Antenna and mechanical switch model.

switch terminal) that will maximize the power output to one IC (when the switch is activated) and minimize the power output to the other IC. Additionally, when the switch is deactivated, the matching networks should operate to match the ICs in the reverse fashion.

Our antenna's simulation results agree well with the measured ones, as shown in Fig. 6. Therefore, the simulated data for our antenna is used for our sensor's system modeling and design. Specifically, our antenna's simulated 1-port model along with the measured 3-port model of the switch (for the case when the switch is activated and when it is deactivated) are exported to ANSYS Circuit Designer. The remaining terminals of the switch are connected to 50Ω ports (i.e., ports A and B) as shown in Fig. 9. Using this model in ANSYS Circuit Designer, the impedances (with the antenna and switch) at ports 2 and 3 can be found for both switch states (i.e., activated and deactivated). This provides the needed information for designing the corresponding matching networks.

Firstly, the impedance at port 2 is measured for when the switch is activated. This impedance is then matched to the conjugate of the RFID IC 2 using a matching network. When the switch is deactivated, the impedance at port 2 will significantly change thereby deteriorating the matching. Therefore, no power will reach RFID IC 2 when the switch is in the deactivated state and will remain OFF (as intended). The

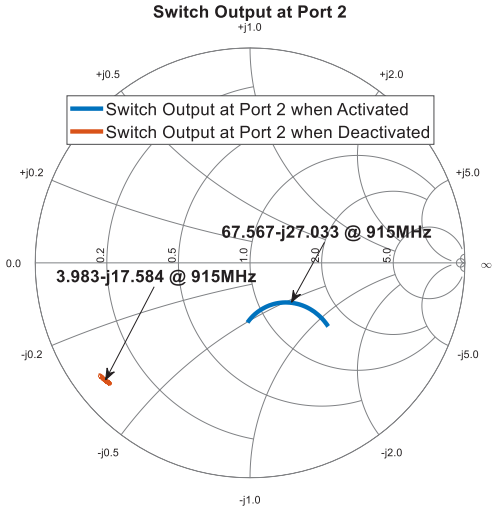

FIGURE 10. Input impedance at port 2 for switch in activated and deactivated states.

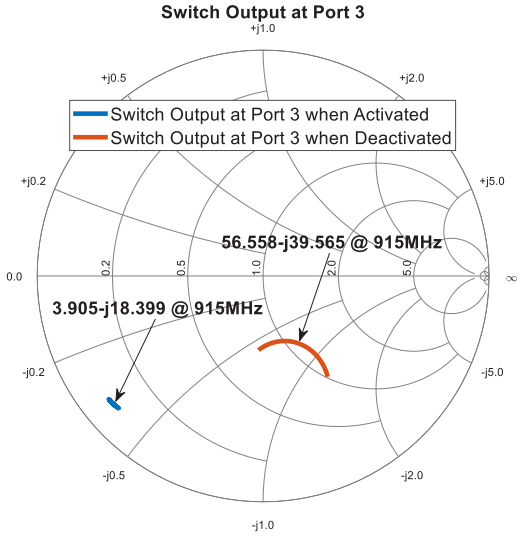

FIGURE 11. Input impedance at port 3 for switch in activated and deactivated states.

impedances at port 2 for both activated and deactivated cases are shown in Fig. 10, and they are indeed very different.

In the deactivated case, we have indicated that little power will be transferred to the IC at port 2; however, at port 3 we seek to maximize the power transfer. The impedance at port 3 is measured for when the switch is deactivated using our circuit model shown in Fig. 9. This impedance is then matched to the conjugate of the RFID IC 1 using a matching network. When the switch is activated, the impedance at port 3 will significantly change thereby deteriorating the matching. Therefore, no power will reach RFID IC 1 when the switch is in the activated state and will remain OFF (as intended). The impedances at port 3 for both activated and deactivated cases are shown in Fig. 11, and they are indeed very different. The final design layout with the antenna, switch, and designed matching networks are depicted in Fig. 12.

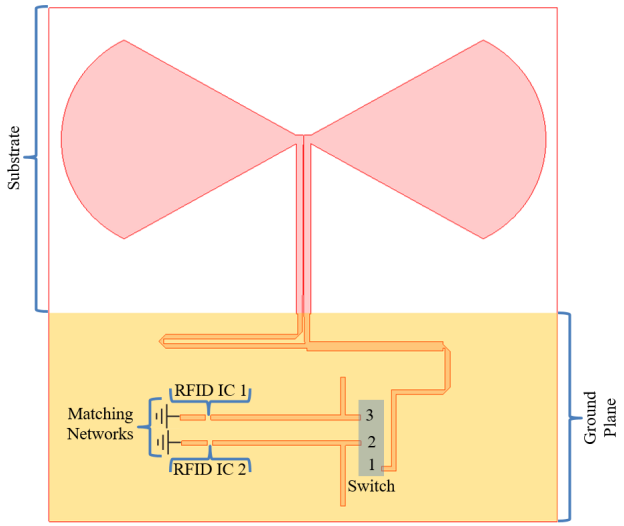

FIGURE 12. RFID sensor design layout.

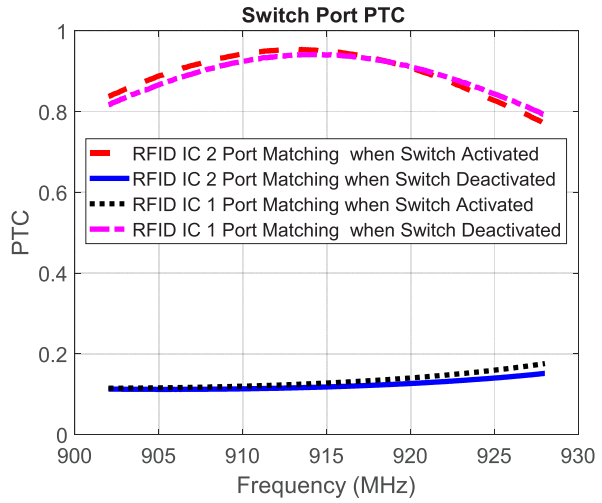

FIGURE 13. Simulated Power Transmission Coefficient (PTC) at the ports where RFID ICs 1 and 2 will be connected, as shown in Fig. 12.

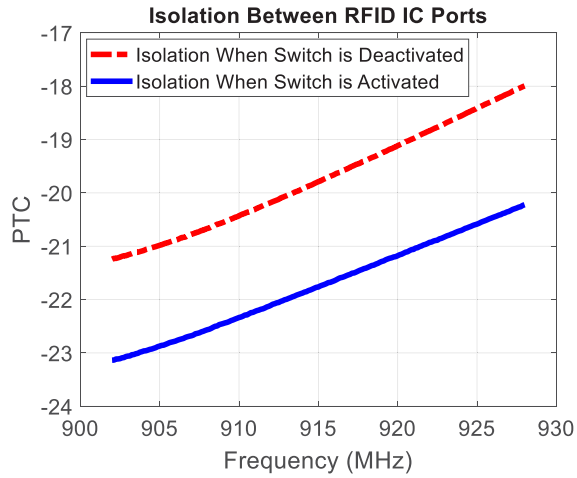

FIGURE 14. Isolation between RFID IC 1 port and RFID IC 2 port.

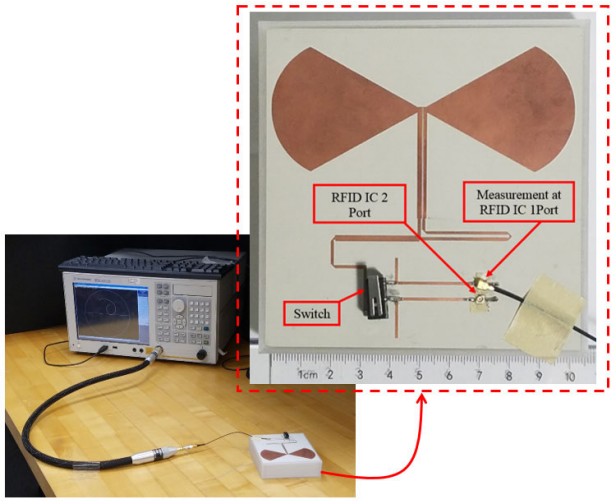

FIGURE 15. Test setup with fabricated prototype for impedance measurements at the ports where the RFID ICs are connected.

Furthermore, to test the degree of matching between each switch port and the RFID IC, we utilize the power transmission coefficient (PTC or τ; $0 \leq \tau \leq 1$) as discussed in [27]. In the case when $\tau = 1$, a conjugate match $\left(Z_{port} = Z_{IC}^{*}\right)$ is obtained that provides maximum power transfer to the IC [50, p. 78]. Fig 13 shows the PTC for both switch states at the two ports, where the RFID ICs 1 and 2 will be connected as per Fig. 12. These results clearly illustrate the following: (a) when the switch is activated, RFID IC 2 (at port 2 of the switch, refer to Fig. 9) will be ON and RFID IC 1 (at port 3 of the switch, refer to Fig. 9) will be OFF, and (b) when the switch is deactivated, RFID IC 2 (at port 2 of the switch, refer to Fig. 9) will be OFF and RFID IC 1 (at port 3 of the switch, refer to Fig. 9) will be ON.

VI. MEASUREMENTS OF SWITCHING CAPABILITY

In this section, a prototype model of our sensor is first fabricated. Then, it is measured using a VNA to validate our sensor's capability to switch the power flow from one RFID IC to the other, as predicted by our simulation results in Fig. 13. The measurements are conducted as follows: the input impedance at the RFID IC 1 port is measured while the RFID IC 2 port is left open (see Fig. 12). The RFID IC 2 port can be left open because the isolation between the two ports is significant (i.e., >18 dB) irrespective of the switch activation status, as shown in Fig. 14.

Fig. 15 shows the test setup and the fabricated prototype. An IPX interface is used to measure the impedance of RFID IC 1 port for both switch states (i.e., activated and deactivated) while RFID IC 2 port is open. These measurements are depicted in Fig. 16. Moreover, the corresponding PTCs are plotted in Fig. 17. According to Figs. 16 and 17, the measured and simulated impedance at RFID IC 1 port agree very well. These results indicate good matching when the switch is deactivated and the intentional degradation in the matching when the switch is activated. Also, Fig. 17 shows that when

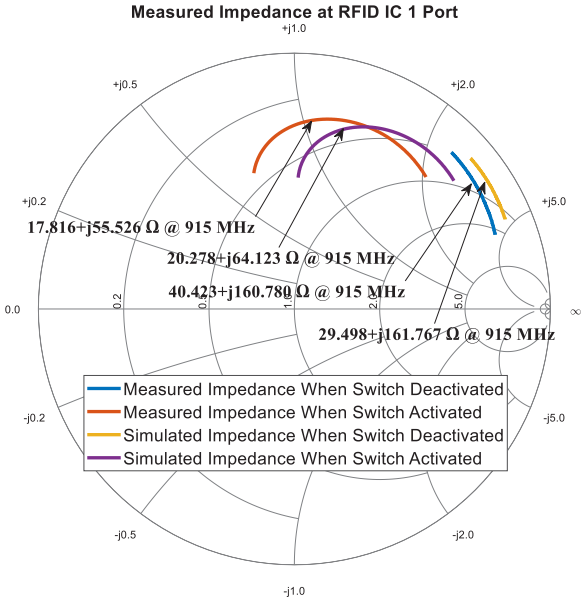

FIGURE 16. Simulated and measured input impedances at RFID IC 1 port.

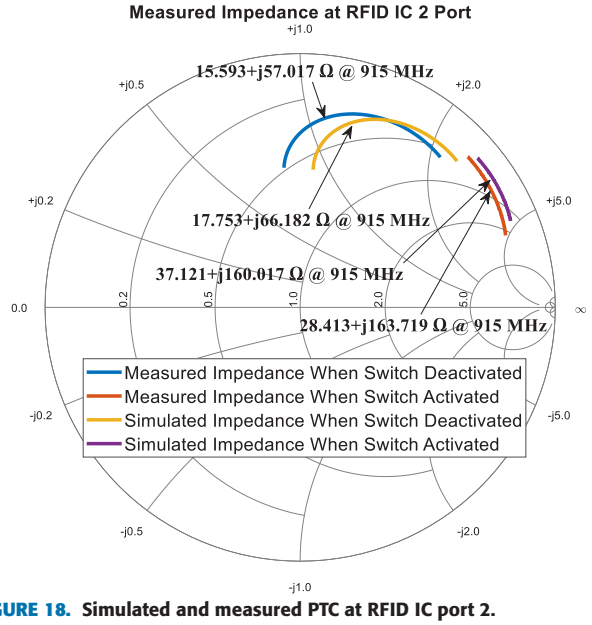

FIGURE 18. Simulated and measured PTC at RFID IC port 2.

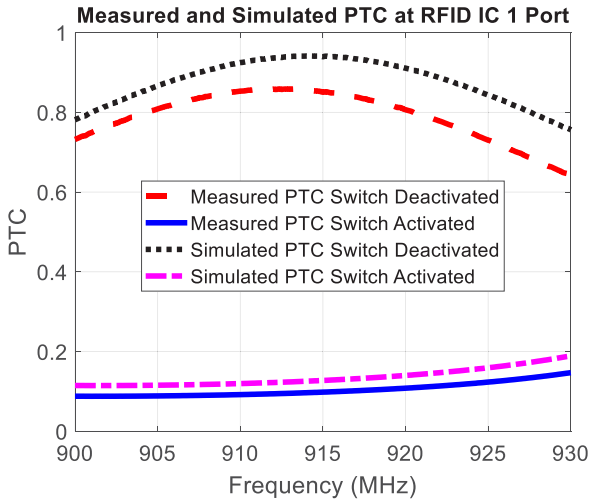

FIGURE 17. Simulated and measured PTC at RFID IC port 1.

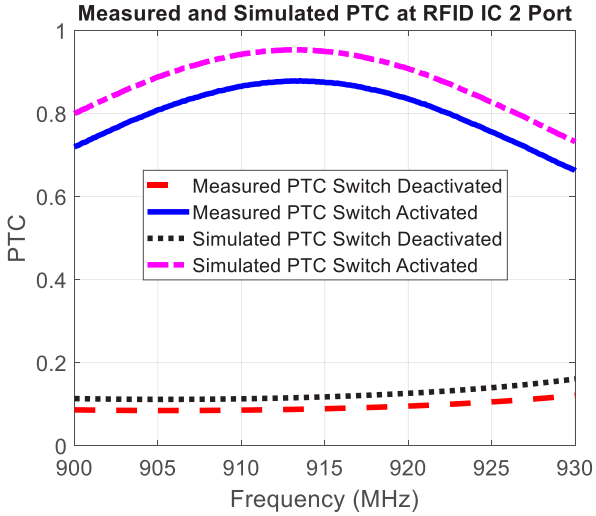

FIGURE 19. Simulated and measured PTC at RFID IC port 2.

the switch is activated and deactivated, the power flow to RFID IC 1 is minimized and maximized, respectively.

To further examine the power-flow switching capability of our design, the same test is conducted for RFID IC 2 port. Namely, the measurements are performed at RFID IC 2 port with RFID IC 1 port open. The simulated and measured results for this case are depicted in Fig. 18. Furthermore, the corresponding PTCs are plotted in Fig. 19. It is clearly seen from these results that the measurements agree well with simulations and confirm the intended operation of our design. Specifically, when the switch is deactivated and activated, the power flow to RFID IC 2 is minimized and maximized, respectively.

VII. VALIDATION OF TEMPERATURE SENSOR

The final design of our sensor is depicted in Fig. 20. The mechanical switch has been fitted with a customized housing consisting of two parts. The first part is a stationary housing,

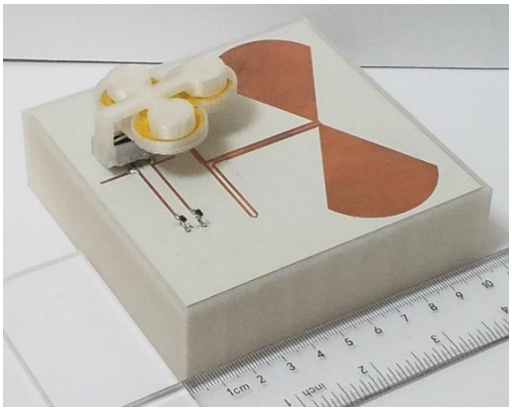

FIGURE 20. RFID temperature sensor with cold-responsive LCE.

which is anchored to the base of the switch. The second part consists of a platform to support the LCE array and is

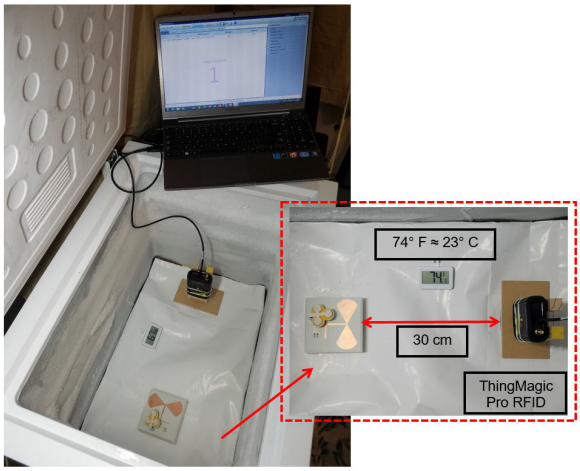

FIGURE 21. RFID temperature sensor with RFID reader inside freezer at room-temperature.

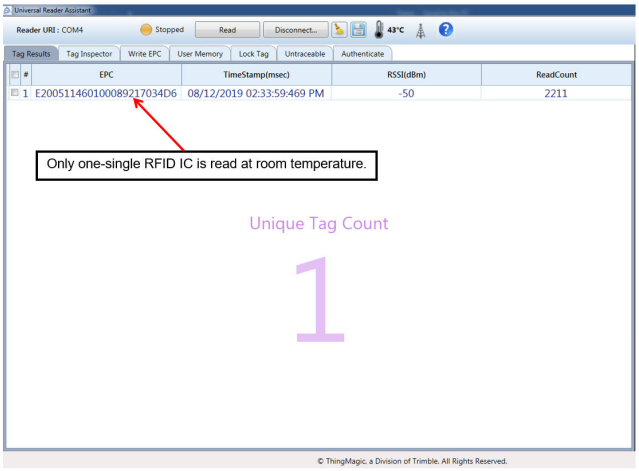

FIGURE 22. Only RFID IC 1 is read at room temperature.

situated on the lever of the switch. When the environmental temperature is lower or equal than approximately −10° C, the LCE is activated (i.e., cold-responsive LCE) and it pushes against the stationary housing and triggers the switch. When the environmental temperature rises and becomes larger than approximately −10° C, the LCE returns to its relaxed state and the switch returns to its original position on its own.

The operating temperature range of the Alien Higgs III RFID IC, which was used in our sensor, is −50° C to 85°C [51]. Therefore, the performance of this IC is unaffected by the temperature conditions that our sensor is exposed to during our experimentations. Also, this RFID IC should perform with no issues in practical applications as the preservation temperatures for perishable goods between −1° C and 10° C are well within the IC's operating temperature range. Additionally, the temperature sensing ability of our RFID passive sensor is tested using the ThingMagic RFID reader as detailed here. The test setup is depicted in Fig. 21. To distinguish which RFID ICs are read during the different stages of our test, the ''Tag Aging'' feature is activated in the RFID reader's software. This feature highlights in gray any unreadable tags within the read range of the reader. Initially, the sensor is placed inside a non-operating freezer. Therefore, the inside volume of the freezer is at room temperature (i.e., 23° C). Since our cold-responsive LCE is not activated at such temperatures, the switch is also not activated and the RFID reader senses only the ID of RFID IC 1, as shown in Fig. 22.

Subsequently, the RFID reader is removed from the freezer while our sensor stays inside the freezer. Then, the freezer is shut and turned on. Due to its chemical composition, our LCE array was designed to actuate at approximately −10 °C. In other words, −10 °C serves as the minimum required temperature to achieve full actuation. The temperature during experimentation was exceeded (i.e., −15 °C) to ensure the LCE has been actuated. Furthermore, this colder temperature allowed for a time window (until the temperature rises above −10 °C) to conduct our RFID measurements as the

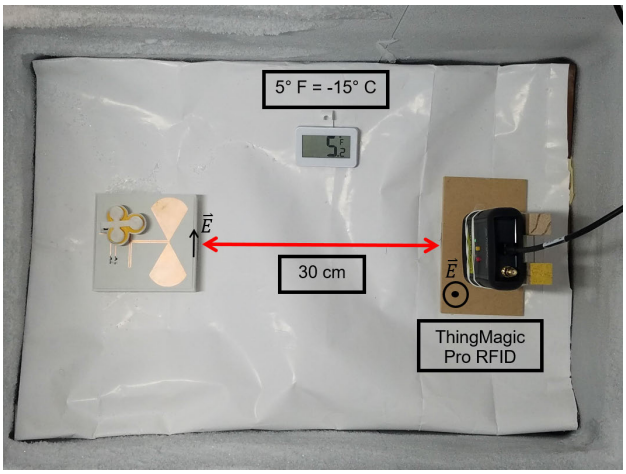

FIGURE 23. RFID temperature sensor with RFID reader inside freezer at −15° C. The sensor and reader are arranged in a "worst case" scenario with perpendicular (polarization) antenna alignment with respect to one another.

measurements were conducted with the freezer door open with the sensor exposed to the ambient room temperature. The RFID reader was then reinserted into the freezer as shown in Fig. 23. In this case, we see that due to the cold temperature the cold-responsive LCE has activated the switch and only the ID of RFID IC 2 is read, as shown in Fig. 24. The ID of RFID IC 1 is clearly highlighted in gray, which means it is not detected by the reader. Moreover, the software also shows that two unique tags were detected (with two different EPCs) within the total time-duration of our test.

Furthermore, our sensor and the reader were oriented in a ''worst case'' scenario; that is, they were positioned so that their antennas are perpendicularly polarized with respect to each other (the E-field polarizations are labelled in Fig. 23). As a result, 30 cm is the largest distance at which the RFID reader can recognize our sensor in this setup (see Fig. 23). However, the read distance can be greatly improved by aligning the polarization of the antennas on our tag with the

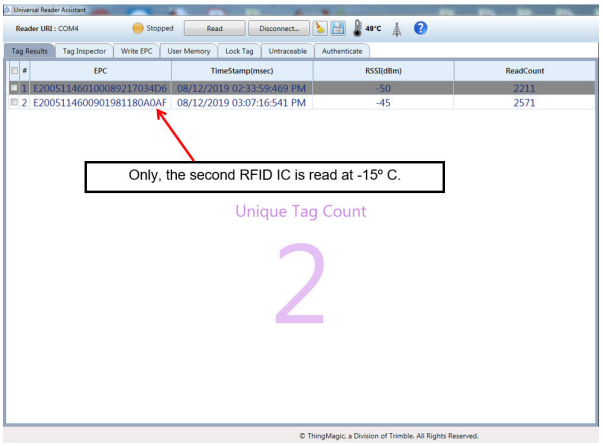

FIGURE 24. Only RFID IC 2 is read at −15° C.

RFID reader. To demonstrate this, we utilize the Polarization Loss Factor (PLF) which accounts for the loss due to the polarization misalignment between the two antennas. The PLF equates to $|\cos\psi|^2$, where ψ defines the difference in the polarization angles between the reader and the sensor antennas (i.e., 90° in Figs. 21 and 23) [39, pg. 71]. For angles approaching 90°, the PLF equates to a loss of approximately 31.6 dB or 0.0006 in linear scale. Moreover, using Friis transmission equation, from [39, pg. 89], the read-range distance, R, between two antennas can be resolved as:

$$R = \frac{1}{4\pi}\sqrt{\frac{P_T}{P_R}G_T G_R \lambda^2 |\cos\psi|^2 PTC_T PTC_R} \qquad (1)$$

where P_T, P_R, G_T, G_R, λ, PTC_T, and PTC_R, represent the transmit power of the RFID reader (30 dBm or 1 W), the received power or the sensitivity of the RFID IC (−18 dBm or 0.000016 W [21]), the gain of the reader antenna that is a half-wave dipole (2.15 dBi or 1.64), the gain of the sensor antenna which from Fig. 4 is 4.6 dBi or 2.88, the wavelength (λ) is 0.328 m, the matching efficiency of the reader transmitter to the antenna (PTC_T) is 100% or 1, and the matching efficiency (PTC_R) of the sensor antenna to the load which from Figs. 17 and 19 equates to approximately 80% or 0.8, respectively. Substituting these values into (1) provides the read-range distance of approximately 31 cm, which agrees well with the measured distance of 30 cm (with only 3% error). This proves the parameter values that we have utilized are correct. Hence, if we redo this calculation assuming the reader antenna and the sensor antenna are now perfectly aligned (i.e., $|\cos\psi|^2 = 1$), the range or distance increases by a factor of approximately 30. Finally, our results show that this design has potential to be utilized in the cold supply chain in terms of its read-range distance. Furthermore, as mentioned in the introduction, we envision each delivery vehicle to be equipped with an RFID wireless reader. Therefore, these readers are stationary and high gain antennas can be utilized to increase the Effective Isotropic Radiated Power (EIRP) and effectively increase the read range. Also, these readers can be equipped with circularly polarized antennas in which the PLF will not exceed 3 dB [52].

In addition, to show consistency in our experiment, Figs. 22 and 24 are time-stamped. Finally, once the freezer is turned off and the temperature returns to room temperature (i.e., 23°C), the LCE returns to its relaxed state and the switch is deactivated. In this case, the RFID reader returns to reading only RFID IC 1 as shown in Fig. 22. The developed sensor was tested with many temperature cycles (i.e., room-to-cold and cold-to-room temperature cycles) as described in the procedure above with consistent successful results. Therefore, our experiment clearly proves that our passive RFID sensor is a not a single-use sensor. In fact, our sensor provides continuous and independent temperature monitoring and detects multiple temperature threshold crossings from cold to room temperature and vice versa. This performance of the developed sensor is reliable because LCEs have shown to provide stable operation over a wide range of temperatures; however, like all materials, thermal degradation can occur at extreme temperatures. LCEs of similar chemistry were found to undergo significant degradation above 300° C [53]. In practice, we have observed fully recovered properties when heating to temperatures as high as 200° C for moderate periods of time. For temperatures below 100° C, degradation is not expected even after long exposure times. If thermal degradation does occur the shape change of the material would become partially irreversible and this would change the threshold for switch activation in our design.

In addition to the successful test results discussed above, the sensor is compact and due to its battery-free operation it has low cost and long operational life. As a result, it can be easily installed to numerous items of various sizes. Therefore, issues regarding malfunctioning refrigeration equipment and operator error, such as, improperly placed items during loading, inadequate packaging, constantly opening and/or leaving the container doors open, and failure to pre-cool the container before loading, can now be detected (and no longer be overlooked) as each item can be constantly monitored. Finally, since each individual item has a sensor attached to it, issues at the cargo-docks are resolved because a form of temperature monitoring is now available due to this sensor.

Finally, the temperature at which Liquid Crystal Elastomers (LCEs) respond to can be adjusted by modifying their chemical composition. For example, in [27], a 4D printed high temperature reactive LCE array was utilized to design a novel temperature sensor. The design presented here is the first sensor that uses cold-responsive LCEs to convey temperature threshold crossings by switch operation between two RFID ICs and it serves as a proof-of-concept for passive detection of cold temperatures (i.e., at −10° C). Consequently, LCEs that react to other temperatures can also be inserted in this sensor to adjust its operating temperature. Furthermore, as mentioned in Section I, the range of preservation temperatures of perishable items, such as, meats, fruits, vegetables, insulin and vaccines, is from −1° C to 10°C. Since the developed sensor's triggering temperature

point is customizable based on the LCE, each item could have a separate sensor configured to trigger at a specific temperature. To conclude, this sensor operates with a binary functionality; that is, the operation of the sensor switches between the operation of two RFID ICs (two Electronic Products Codes) depending on whether a temperature threshold has been crossed or not. Future work could pursue designs that are able to detect three different ranges and they would need new LCE designs to be developed.

VIII. CONCLUSION

In this work, we focused on developing a new temperature sensor design that serves as a proof of concept for sensors that integrate novel LCEs, antenna systems, and RF circuits, to reversibly and reliably convey temperature threshold crossings. Specifically, we have developed a sensor that conveys changes in temperature by switching its operation between two unique RFID ICs. Therefore, our sensor detects temperature threshold crossing in a very clear and robust manner, i.e., at cold temperature one RFID IC ID is read and at room temperatures another RFID IC ID is read. Our sensor uses novel cold-reactive liquid crystal elastomers that operate reversibly. Hence, this sensor can autonomously operate through multiple room-to-cold and cold-to-room temperature cycles in real-time. Also, our sensor has a battery-free operation (i.e., it is purely passive). In fact, this is the first temperature sensor that operates by switching between two RFID ICs (based on temperature) using cold-responsive liquid crystal elastomers.

For this sensor, we designed a wideband bow-tie antenna, which operates in the UHF RFID band of 902-928 MHz. The antenna was fed with a CPS to microstrip transmission line conversion. A balun was also designed using a pair of feedlines 180° out of phase, which are matched to 50Ω using a quarter-wave transformer.

A three-port model of the mechanical switch was developed using 3 two-port measurements. This model was used with the antenna model to design matching networks, that maximize power transfer to one RFID IC while minimizing the power to the other IC when the switch is activated and visa-versa when the switch is deactivated.

A custom housing and platform were also designed to translate the actuation of the LCE array to the switch without any external intervention (i.e., automatic resetting) as follows: activate the switch when the LCE is stimulated (i.e., at cold temperatures) and deactivate the switch when the stimulus is removed (i.e., at room temperature). The battery-free and autonomous functionality of this sensor makes it a robust option for temperature monitoring in the CSC.

REFERENCES

[1] (Mar-2018). *Cold Chain—Why Is It Growing So Fast? The Logistics of Logistics*. Accessed: Oct. 20, 2018. [Online]. Available: https://www.thelogisticsoflogistics.com/cold-chain-growing-fast/

[2] (2016). *2016 Top Markets Report Cold Supply Chain*. Accessed: Oct. 28, 2019. [Online]. Available: https://www.trade.gov/topmarkets/pdf/Cold_Chain_Top_Markets_Report.pdf

[3] A. Dada and F. Thiesse. (2018). *Sensor Applications in the Supply Chain: The Example of Quality-Based Issuing of Perishables*. Accessed: May 14, 2018. [Online]. Available: https://rd.springer.com/content/pdf/10.1007%2F978-3-540-78731-0_9.pdf

[4] *Cold Chain Logistics, Cold Supply Chain|Cold Chain Management*. Accessed: Oct. 20, 2018. [Online]. Available: https://www.parexel.com/solutions/clinical-research/clinical-trial-supplies-and-logistics/cold-chain-logistics

[5] (2008). *Protecting Perishable Foods During Transport by Truck*. Accessed:May 5, 2018. [Online]. Available: https://www.ams.usda.gov/sites/default/files/media/TransportPerishableFoodsbyTruck%5B1%5D.pdf

[6] (2001). *Recommendations on the Control and Monitoring of Storage and Transportation Temperatures of Medicinal Products*. Accessed: May 5, 2018. [Online]. Available: https://temptrust.mesalabs.com/wp-content/uploads/sites/47/2012/05/MHRAcon007569.pdf

[7] R. Bhattacharyya, C. Floerkemeier, S. Sarma, and D. Deavours, "RFID tag antenna based temperature sensing in the frequency domain," in *Proc. RFID*, Orlando, FL, USA, Apr. 2011, pp. 70–77.

[8] United World Transportation. (2018). *The 4 Most Common Cold Chain Logistics Problems Truckers Face and Tips for Solving Them*. Accessed: May 6, 2018. [Online]. Available: https://unitedworldtransportation.com/4-common-cold-chain-logistics-problems-truckers-face-tips-solving/

[9] R. Bhattacharyya, C. Floerkemeier, and S. Sarma, "RFID tag antenna based temperature sensing," in *Proc. RFID*, Orlando, FL, USA, Apr. 2010, pp. 8–15.

[10] U. Facts. (2018). *Topic: Organic Food Industry*. Accessed: May 14, 2018. [Online]. Available: https://www.statista.com/topics/1047/organic-food-industry/

[11] D. Dobkin, *The RF in RFID*, 1st ed. Amsterdam, The Netherlands: Elsevier, 2008.

[12] P. Kumar, H. W. Reinitz, J. Simunovic, K. P. Sandeep, and P. D. Franzon, "Overview of RFID technology and its applications in the food industry," *J. Food Sci.*, vol. 74, no. 8, pp. R101–R106, Oct. 2009.

[13] (2020). *SENSOR TEMPERATURE DOGBONE—RFID—Smartrac*. Accessed: Mar. 24, 2020. [Online]. Available: https://www.smartrac-group.com/sensor-temperature-dogbone.html

[14] (2020). *Freshtimeá Tags Infratab-Dev*. Accessed: Mar. 24, 2020. [Online]. Available: https://infratab-dev.myshopify.com/collections/freshtime-tags

[15] (2020). *Rfidjournal*. Accessed: Mar. 24, 2020. [Online]. Available: http://www.rfidjournal.net/masterPresentations/live2009/np/Finalist_IDS_Microship.pdf

[16] (2020). *SL900A EPC Class 3 Sensory Tag Chip—For Automatic Data Logging*. Accessed: Mar. 23, 2020. [Online]. Available: https://ams.com/documents/20143/36005/SL900A_DS000294_5-00.pdf/d399f354-b0b6-146f-6e98-b124826bd737

[17] (2020). *EPC Sensor Tag and Data Logger IC—ams SL900A|ams*. Accessed: Mar. 24, 2020. [Online]. Available: https://ams.com/sl900a#tab/documents

[18] C. Occhiuzzi and G. Marrocco, "Constrained-design of passive UHF RFID sensor antennas," *IEEE Trans. Antennas Propag.*, vol. 61, no. 6, pp. 2972–2980, Jun. 2013.

[19] C. Occhiuzzi, S. Caizzone, and G. Marrocco, "Passive UHF RFID antennas for sensing applications: Principles, methods, and classifcations," *IEEE Antennas Propag. Mag.*, vol. 55, no. 6, pp. 14–34, Dec. 2013, doi: 10.1109/MAP.2013.6781700.

[20] G. Marrocco, "Pervasive electromagnetics: Sensing paradigms by passive RFID technology," *IEEE Wireless Commun.*, vol. 17, no. 6, pp. 10–17, Dec. 2010.

[21] J. Virtanen, L. Ukkonen, T. Bjorninen, L. Sydanheimo, and A. Z. Elsherbeni, "Temperature sensor tag for passive UHF RFID systems," in *Proc. IEEE Sensors Appl. Symp.*, San Antonio, TX, USA, Feb. 2011, pp. 312–317.

[22] K. Dong, F. Yang, S. Xu, and M. Li, "Dual-frequency reconfigurable patch antenna with thermal switches for temperature monitoring," in *Proc. URSI Int. Symp. Electromagn. Theory (EMTS)*, Espoo, Aug. 2016, pp. 118–120.

[23] A. A. Babar, S. Manzari, L. Sydanheimo, A. Z. Elsherbeni, and L. Ukkonen, "Passive UHF RFID tag for heat sensing applications," *IEEE Trans. Antennas Propag.*, vol. 60, no. 9, pp. 4056–4064, Sep. 2012.

[24] G. Marrocco, L. Mattioni, and C. Calabrese, "Multiport sensor RFIDs for wireless passive sensing of objects—basic theory and early results," *IEEE Trans. Antennas Propag.*, vol. 56, no. 8, pp. 2691–2702, Aug. 2008.

[25] S. Caizzone, C. Occhiuzzi, and G. Marrocco, "Multi-chip RFID antenna integrating shape-memory alloys for detection of thermal thresholds," *IEEE Trans. Antennas Propag.*, vol. 59, no. 7, pp. 2488–2494, Jul. 2011.
[26] Y. Shafiq, J. Henricks, C. P. Ambulo, T. H. Ware, and S. V. Georgakopoulos, "A passive RFID temperature sensing antenna with liquid crystal elastomer switching," *IEEE Access*, vol. 8, pp. 24443–24456, 2020.
[27] Y. Shafiq, J. S. Gibson, H. Kim, C. P. Ambulo, T. H. Ware, and S. V. Georgakopoulos, "A reusable battery-free RFID temperature sensor," *IEEE Trans. Antennas Propag.*, vol. 67, no. 10, pp. 6612–6626, Oct. 2019, doi: 10.1109/TAP.2019.2921150.
[28] J. S. Gibson, X. Liu, S. V. Georgakopoulos, J. J. Wie, T. H. Ware, and T. J. White, "Reconfigurable antennas based on self-morphing liquid crystalline elastomers," *IEEE Access*, vol. 4, pp. 2340–2348, 2016.
[29] T. J. White and D. J. Broer, "Programmable and adaptive mechanics with liquid crystal polymer networks and elastomers," *Nature Mater.*, vol. 14, no. 11, pp. 1087–1098, Nov. 2015.
[30] J. Küpfer and H. Finkelmann, "Nematic liquid single crystal elastomers," *Die Makromolekulare Chem., Rapid Commun.*, vol. 12, no. 12, pp. 717–726, 1991.
[31] T. H. Ware, M. E. McConney, J. J. Wie, V. P. Tondiglia, and T. J. White, "Voxelated liquid crystal elastomers," *Science*, vol. 347, no. 6225, pp. 982–984, Feb. 2015.
[32] C. P. Ambulo, J. J. Burroughs, J. M. Boothby, H. Kim, M. R. Shankar, and T. H. Ware, "Four-dimensional printing of liquid crystal elastomers," *ACS Appl. Mater. Interface*, vol. 9, no. 42, pp. 37332–37339, Oct. 2017.
[33] A. Kotikian, R. L. Truby, J. W. Boley, T. J. White, and J. A. Lewis, "3D printing of liquid crystal elastomeric actuators with spatially programed nematic order," *Adv. Mater.*, vol. 30, no. 10, Mar. 2018, Art. no. 1706164.
[34] M. López-Valdeolivas, D. Liu, D. J. Broer, and C. Sánchez-Somolinos, "4D printed actuators with soft-robotic functions," *Macromolecular Rapid Commun.*, vol. 39, no. 5, Mar. 2018, Art. no. 1700710.
[35] C. D. Modes, K. Bhattacharya, and M. Warner, "Disclination-mediated thermo-optical response in nematic glass sheets," *Phys. Rev. E, Stat. Phys. Plasmas Fluids Relat. Interdiscip. Top.*, vol. 81, no. 6, Jun. 2010.
[36] T. Bjorninen, M. Lauri, L. Ukkonen, R. Ritala, A. Z. Elsherbeni, and L. Sydanheimo, "Wireless measurement of RFID IC impedance," *IEEE Trans. Instrum. Meas.*, vol. 60, no. 9, pp. 3194–3206, Sep. 2011.
[37] K. RamaDevi, A. M. Prasad, and A. J. Rani, Design of RFID Tag Antennas at UHF Band with Different Materials, 1st ed. Beau-Bassin, Mauritius: LAMBERT Academic Publishing, 2018, p. 53.
[38] (2019). *D2F Ultra Subminiature Basic Switch*. Accessed: Feb. 7, 2019. [Online]. Available: https://media.digikey.com/pdf/Data%20Sheets/Omron%20PDFs/D2F_0318_DS.pdf
[39] C. Balanis, *Antenna Theory*. 4th ed. Hoboken, NJ, USA: Wiley, 2016
[40] J. Kraus and R. Marhefka, *Antennas for All Applications*. 3rd ed. Boston, MA, USA: McGraw-Hill, 2003, pp. 380–387.
[41] C. Paul, *Introduction to Electromagnetic Compatibility*. 2nd ed. Hoboken, NJ, USA: Wiley, 2006, p. 460.
[42] Y. Qian and T. Itoh, "A broadband uniplanar microstrip-to-CPS transition," in *Proc. Asia–Pacific Microw. Conf.*, 1997, pp. 1–6.
[43] N. Kaneda, Y. Qian, and T. Itoh, "A broad-band microstrip-to-waveguide transition using quasi-yagi antenna," *IEEE Trans. Microw. Theory Techn.*, vol. 47, no. 12, pp. 2562–2567, Dec. 1999.
[44] L. Yuan and W. Tang, "Novel miniaturized broadband Quasi-Yagi antennas based on modified Bowties driver for wireless technology applications," *Prog. Electromagn. Res.*, vol. 63, pp. 151–161, 2018.
[45] A. Eldek, A. Elsherbeni, and C. Smith, "Wideband microstrip-fed printed bow-tie antenna for phased-array systems," *Microw. Opt. Technol. Lett.*, vol. 43, no. 2, pp. 123–126, 2004.
[46] R. Garg, I. Bahl, and M. Bozzi, *Microstrip Lines and Slotlines*. Norwood, MA, USA: Artech House, 1979, pp. 257–280.
[47] (2019). *TMM Thermoset Microwave Materials*. Accessed: Nov. 4, 2019. [Online]. Available: https://rogerscorp.com/-/media/project/rogerscorp/documents/advanced-connectivity-solutions/english/data-sheets/tmm-thermoset-laminate-data-sheet-tmm3-tmm4-tmm6-tmm10-tmm10i-tmm13i.pdf
[48] (2009). *Management of Reusable Plastic Crates in Fresh Produce Supply Chains*. Accessed: Feb. 13, 2020. [Online]. Available: http://www.fao.org/3/a-i0930e.pdf
[49] (2019). *D2F Ultra Subminiature Basic Switch*. Accessed: Feb. 7, 2019. [Online]. Available: https://media.digikey.com/pdf/Data%20Sheets/Omron%20PDFs/D2F_0318_DS.pdf
[50] D. M. Pozar, *Microwave Engineering*, 4th ed. Hoboken, NJ, USA: Wiley, 2011.
[51] (2013). *Higgs 3 IC Datasheet Supplement*. Accessed: Feb. 11, 2020. [Online]. Available: https://www.rfid-alliance.com/RFIDshop/Alien-Technology-Higgs-3-IC-Datasheet.pdf
[52] K. Blattenberger. *Electronic Warfare and Radar Systems Engineering Handbook—Polarization Electronic Warfare and Radar Systems Engineering Handbook—Polarization—RF Cafe*. Accessed: Mar. 23, 2020. [Online]. Available: https://www.rfcafe.com/references/electrical/ew-radar handbook/polarization.htm
[53] Z. Wang, H. Tian, Q. He, and S. Cai, "Reprogrammable, reprocessible, and self-healable liquid crystal elastomer with exchangeable disulfide bonds," *ACS Appl. Mater. Interface*, vol. 9, no. 38, pp. 33119–33128, Sep. 2017.

YOUSUF SHAFIQ (Member, IEEE) received the B.S. and M.S. degrees in electrical engineering from Florida International University (FIU), Miami, in 2009 and 2010, respectively, where he is currently pursuing the Ph.D. degree in electrical engineering.

From 2010 to 2012, he worked as a Communications Systems Engineer with Lockheed Martin Space Systems, Newtown, PA. Subsequently, he worked as an RCS Engineer at Pratt and Whitney, West Palm Beach, FL. Finally, from 2014 to 2017, he was an Electrical Engineer with the Naval Surface Warfare Center, Panama City Beach, FL. In 2017, he became a Research Assistant with the RFCOM Lab, Florida International University to complete his Ph.D. degree in electrical engineering. His research area consisted of wireless sensing using innovative reactive materials combined with novel antenna and RF circuit design techniques.

JULIA HENRICKS received her B.S. degree in Biomedical Engineering from The University of Texas at Dallas in 2018. From 2018 to 2019, she pursued a Ph.D. degree in Biomedical Engineering and worked on light-responsive materials and temperature-responsive materials for antennas and implantable devices. She currently works as a Reliability Engineer at Abbott Laboratories, testing Alinity s blood and plasma screening devices.

CEDRIC P. AMBULO received the B.A. degree in Physics from the Austin College, in 2016. He joined the Ware Research Laboratory, The University of Texas at Dallas, in fall 2016. He is currently researching and developing stimuli-responsive liquid crystal elastomer actuators toward soft robotic applications.

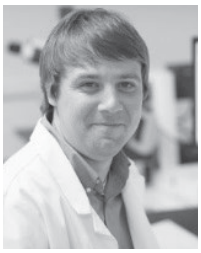

TAYLOR H. WARE received the B.S. degree from the Georgia Institute of Technology, in 2009, and the M.S. and Ph.D. degrees from The University of Texas at Dallas, in 2011 and 2013, respectively. From 2013 to 2015, he was a Postdoctoral Researcher with the Air Force Research Laboratory. Since 2015, he has been an Assistant Professor with the Bioengineering Department, The University of Texas at Dallas. His research interests include liquid crystal materials, flexible electronics, and biomaterials.

STAVROS V. GEORGAKOPOULOS (Senior Member, IEEE) received the Diploma degree in electrical engineering from the University of Patras, Patras, Greece, in June 1996, and the M.S. degree in electrical engineering and the Ph.D. degree in electrical engineering from Arizona State University (ASU), Tempe, in 1998 and 2001, respectively. From 2001 to 2007, he was a Principal Engineer with SV Microwave, Inc. Since 2007, he has been with the Department of Electrical and Computer Engineering, Florida International University, Miami, where he is currently a Professor, the Director of the Transforming Antennas Center (a research center on foldable/origami, physically reconfigurable, and deployable antennas), and the Director of the RF Communications, Millimeter-Waves, and Terahertz Laboratory. His current research interests relate to novel antennas, arrays, RFID, microwave and RF systems, novel sensors and wireless powering of portable, and wearable and implantable devices.

Dr. Georgakopoulos received the 2015 FIU President's Council Worlds Ahead Faculty Award, which is the highest honor FIU extends to a faculty member for excelling in research, teaching, mentorship, and service. He serves as an Associate Editor of the IEEE TRANSACTIONS ON ANTENNAS AND PROPAGATION, from 2013 to 2019, and has been an Associate Editor of the IEEE OPEN JOURNAL OF ANTENNAS AND PROPAGATION, since 2019.